In-vivo pharmacokinetic & biodistribution studies

6. In-vivo Pharmacokinetic and Biodistribution Studies

6.1 Introduction

Colloidal drug carriers such as nanoparticles and liposomes can be used to improve the therapeutic index of both established and new drugs by modifying their distribution, thus increasing their efficiency and/or reducing their toxicity. This is because the drug distribution then follows the carrier, rather than depending on the physicochemical properties of the drug (Muller et al., 2000). The effectiveness of drug delivery systems can be attributed to their small size, reduced drug toxicity to other organs, controlled drug release and modification of drug pharmacokinetics and biodistribution. Tumor vasculature has been described as "leaky" due to the presence of interendothelial junctions and transendothelial channels, which for several tumor models have been reported to have sizes ranging between 0.2 and 1.2 μm (Hobbs et al., 1998; Yuan et al., 1995). Therefore, it has been demonstrated that the use of colloidal systems improves tumor therapy due to enhanced permeability and retention effect (EPR) within the tumor site (Maeda et al., 2000). Targeting ligands can be further attached to the carrier surface to improve therapeutic outcomes via active targeting. Rat models implanted with C6 glioma cells have been widely utilized for assessment of new therapeutic modalities. In the present study male SD rats were subcutaneously implanted with C6 glioma cells. The tumor induced rats were used for pharmacokinetic and biodistribution studies.

6.2 Animals

All experiments were previously approved by the Committee for the Purpose of Control and Supervision of Experiments on Animals (CPCSEA), India. Male Sprague Dawley (SD) rats 4-5 weeks old and weighing 250-300 gms were obtained from Sun Pharma Advanced Research Company Ltd., Vadodara. The animals were acclimatized to the surroundings for a week. Food and water were provided *ad libitum.*

6.3 METHODS

6.3.1 Implantation of tumor cells

One day before the implantation of tumor cells, hair on the backside were removed by shaving. C6 rat glioma cells were harvested by trypsinization and resuspended in growth medium. 5 X 10^6 cells were injected sub-cutaneously into the back of the rats and allowed to grow. Size of the tumor was measured by vernier callipers. The volume of the tumor was calculated as $\frac{1}{2}ab^2$ (a=long diameter, b=short diameter) (Ueda et al., 1994).

6.3.3 Pharmacokinetic and Biodistribution studies

The rats implanted with C6 rat glioma cells were used for pharmacokinetics and biodistribution studies. The animals were anaesthetized with ether. PTX solution and PTX loaded in different NPs formulations was administered intravenously via the tail vein at a dose of 20mg/kg body weight. Each group consisted of 3 animals. The blood samples were collected from the retro-orbital plexus of rat eye, at 0.5, 1,2,4,8,12 and 24 hrs post-injection into anticoagulant (3%w/v sodium citrate solution) treated vials. The collected blood was centrifuged at 3000 rpm for 10 minutes at 4°C in a cooling centrifuge (Sigma, Osterode, Germany) to isolate the plasma. At 1, 2, 4 and 24 hrs post injection rats were euthanized and different organs (liver, spleen, lungs, kidneys, heart and tumor) were isolated and homogenized in distilled water at 5%w/v. The homogenate was centrifuged at 7000rpm for 10 minutes at 4°C in a cooling centrifuge to collect clear tissue homogenate. Isolated plasma was stored at -70°C until analysed. The samples were analysed as described in Analytical methods by HPLC.

6.3.4 Statistical analysis

Pharmacokinetic parameters were calculated using Kinetica®4.4 (Innaphase, Philadelphia, PA, USA) applying non-compartmental kinetics for IV bolus. All data are reported as mean ± SD (standard deviation). Statistical evaluations were made using ANOVA and differences greater than $p<0.05$ were considered significant.

6.4 Results and Discussion

6.4.1 Tumor formation

5 million C6 rat glioma cells were injected into the sub-cutaneous region of SD rats on back side. Tumors were palpable at day 10 which were visible at around 14-15th day in all the rats. The results indicate that the success rate for tumor implantation of C6 glioma cells was 100% in male SD rats. The tumor volume was found to be 751 ± 35 mm^3 at day 15 (n=36).

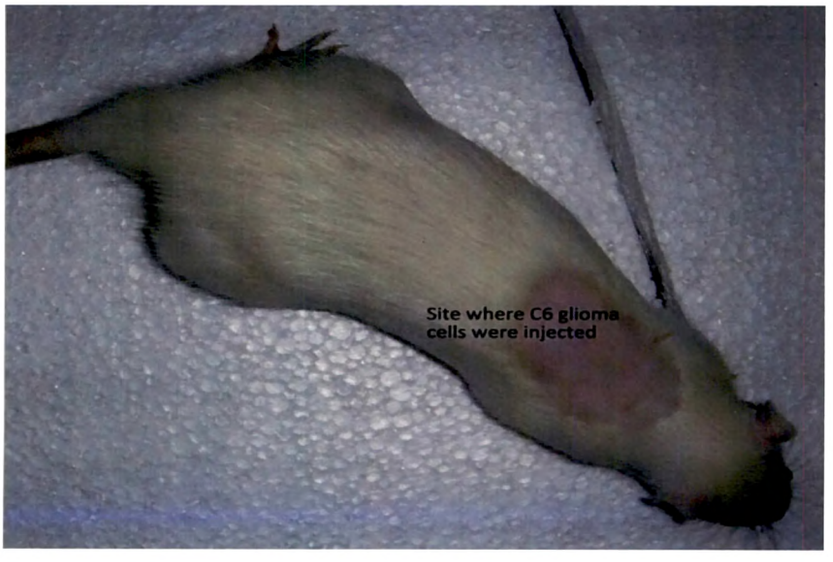

(A)

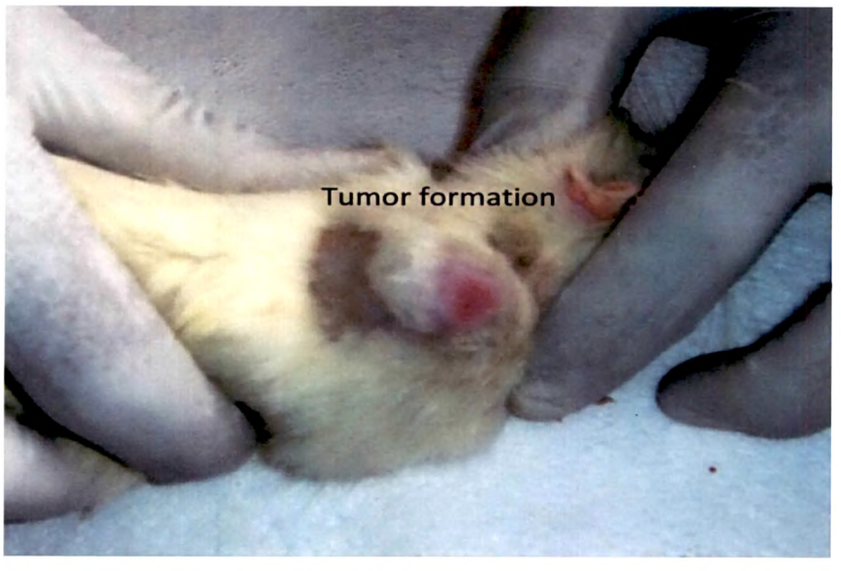

(B)

Figure 6. 1: A) Normal rat B) Rat with a subcutaneous C6 glioma

6.4.2 Pharmacokinetics and Biodistribution

The results of pharmacokinetic and biodistribution of PTX solution and PTX NPs after iv administration in SD rats are presented in Table 1 and 3. The plasma AUC $_{(0\rightarrow 24)}$, AUC $_{(0\rightarrow\infty)}$, MRT and $t_{1/2}$ of PTX solution and NPs are presented in Table 2. Plasma concentration Vs time profiles are shown in Figure 1. Tissue concentration Vs time profiles are shown in Figure 2 (a-f). From the plasma concentration profiles after iv administration it is clearly evident that the PTX in solution form in rapidly cleared from blood whereas, PTX loaded in different NPs formulations are retained in blood for longer time periods indicating the long circulation properties of drug loaded NPs. These findings are indicative of the increased residence time and slower elimination of drug in the form of nanoparticles. This increase in the residence time may be attributed to decreased opsonisation from blood due to smaller size of nanoparticle (≤200nm) (Moghimi et al., 1993) and hydrophilicity of the surface of NPs which imparts stealthiness. Hydroxyl groups of residual PVA on surface of PLGA NP; free -OH groups and Tf on Tf conjugated PLGA NPs (Sahoo et al. 2002), -OH groups of Pluronic®P85 on Pluronic®P85 coated PLGA NPs (Batrakova et al., 2004), -OH groups of Poloxamer 188 on PBCA and GTS SLN (Moghimi et al., 2000) which provides a stealth effect. Significant differences ($P<0.05$) among the results of various pharmacokinetic parameters were observed after i.v. administration of PTX solution and PTX NPs. The plasma $AUC_{(0\rightarrow\infty)}$, MRT and $t_{1/2}$ of PTX loaded into NPs was found to be significantly higher than PTX in solution. The MRT of PTX-PLGA NPs, Pluronic®P85 coated PTX-PLGA NPs, Tf conjugated PTX-PLGA NPs, PTX-PBCA NPs and PTX-GTS SLN was found to be 2.68, 3.0, 3.76, 3.11 and 3.13 folds higher than PTX solution respectively. The high values of MRT and $t_{1/2}$ for NP formulations are indicative of slow clearance and long blood circulation of drug loaded nanoparticles. Also the half-life of PTX increased when PTX was formulated into nanoparticles. The $t_{1/2}$ of PTX in PTX-PLGA NPs, Pluronic®P85 coated PTX-PLGA NPs, Tf conjugated PTX-PLGA NPs, PTX-PBCA NPs and PTX-GTS SLN was found to be 1.88, 2.06, 2.58, 2.10 and 2.15 times higher than PTX in solution. The $AUC_{(0\rightarrow\infty)}$ of PTX in PTX-PLGA NPs, Pluronic®P85 coated PTX-PLGA NPs, Tf conjugated PTX-PLGA NPs, PTX-PBCA NPs and PTX-GTS SLN was found to be 3.34, 3.61, 5.09, 4.06 and 4.2 times higher than PTX in solution.

Table 6. 1: Concentration of PTX in plasma after i.v. administration to rats at dose of 20mg/kg

Time (hrs)	Concentration (µg/mL) ± SD (n=3)					
	PTX solution	PTX PLGA NPs	Pluronic®P-85 coated PTX PLGA NPs	Tf conjugated PTX PLGA NPs	PTX PBCA NPs	PTX GTS SLN
0.5	52.71 ± 1.08	70.2 ± 2.12	68.4 ± 1.65	78.3 ± 1.49	74.1 ± 2.42	73.16 ± 1.27
1	32.76 ± 2.79	51.6 ± 2.97	53.7 ± 2.86	62.5 ± 3.52	59.6 ± 3.58	55.26 ± 2.31
2	14.07 ± 3.12	45.8 ± 2.76	43.2 ± 2.97	56.4 ± 2.69	50.2 ± 3.81	50.27 ± 4.26
4	5.18 ± 1.60	32.7 ± 2.36	30.1 ± 3.48	42.7 ± 3.76	34.9 ± 4.61	41.30 ± 3.24
8	1.12 ± 1.98	15.3 ± 3.76	21.4 ± 1.75	25.3 ± 4.61	19.4 ± 2.96	20.28 ± 3.86
12	0.16 ± 2.17	6.20 ± 3.45	7.60 ± 3.60	12.8 ± 3.87	10.7 ± 3.15	5.70 ± 2.16
24	0.05 ± 2.31	1.01 ± 2.79	0.95 ± 2.85	3.50 ± 3.92	1.60 ± 2.85	1.20 ± 1.98

Table 6. 2: Plasma C_{max}, T_{max}, $AUC_{(0-24)}$, $AUC_{(0-\infty)}$, MRT, $t_{1/2}$ of PTX after i.v. administration to rats at dose of 20mg/kg

Pharmacokinetic parameters	PTX solution	PTX PLGA NPs	Pluronic®P-85 coated PTX PLGA NPs	Tf conjugated PTX PLGA NPs	PTX PBCA NPs	PTX GTS SLN
C_{max} (µg/mL)	52.71	70.2	68.4	78.3	74.1	73.16
T_{max} (h)	0.5	0.5	0.5	0.5	0.5	0.5
$AUC_{(0-24)}$ (h*µgmL^{-1})	107.86	356.74*	383.11*	524.39*	430.05*	443.73*
$AUC_{(0-\infty)}$ (h*µgmL^{-1})	108.23	362.52	391.54	551.83	440.27	455.51
MRT (h)	2.03	5.46*	6.11*	7.64*	6.33*	6.37*
$t_{1/2}$ (h)	2.1	3.96*	4.33*	5.43*	4.42*	4.53*

Table 6. 3: Tumor C_{max}, T_{max}, $AUC_{(0-24)}$, $AUC_{(0-\infty)}$, MRT, $t_{1/2}$ of PTX after i.v. administration to rats at dose of 20mg/kg

Pharmacokinetic parameters	PTX solution	PTX PLGA NPs	Pluronic®P-85 coated PTX PLGA NPs	Tf conjugated PTX PLGA NPs	PTX PBCA NPs	PTX GTS SLN
C_{max} (µg/mL)	13.7	17.58	27.52*	32.53*	24.5*	22.64*
T_{max} (h)	2	2	2	2	2	2
$AUC_{(0-24)}$ (h*µgmL^{-1})	85.52	307.15*	436.36*	585.12*	405.96*	398.51*
$AUC_{(0-\infty)}$ (h*µgmL^{-1})	85.71	580.53*	661.18*	1353.78*	698.34*	763.14*
MRT (h)	4.62	31.72*	22.31*	41.72*	27.49*	32.36*
$t_{1/2}$ (h)	2.67	21.65*	15.18*	28.35*	18.55*	22.19*

(*very significant difference compared to solution, $p<0.0001$)

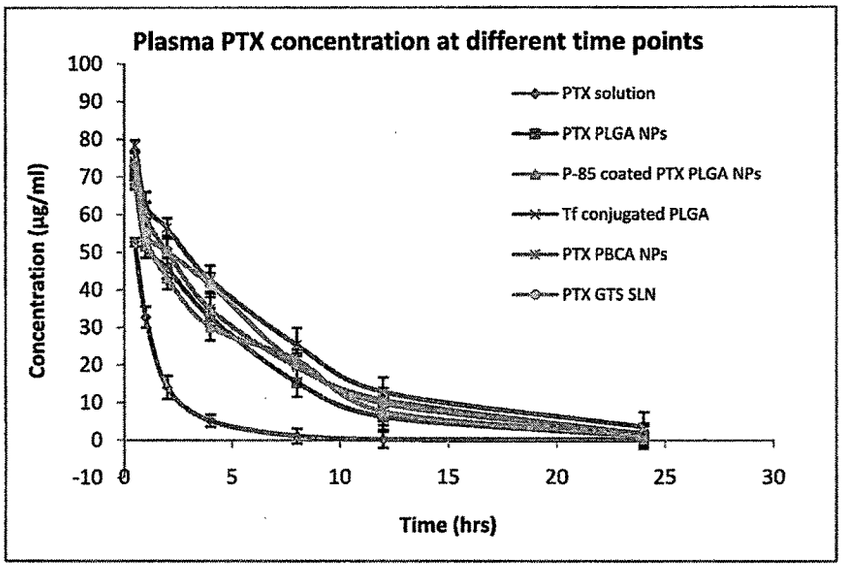

Figure 6. 2: Plasma PTX concentration Vs time profiles for PTX solution and NPs

A major portion of the injected dose was found in the organs of the reticuloendothelial system (RES) i.e. liver, spleen and lungs. The amount of PTX in the liver was found to be less in case of PTX encapsulated into NPs than PTX in solution form. The lower accumulation PTX in the liver in case of nanoparticles compared to solution may be due to the hydrophilicity associated with the nanoparticle surface, as mentioned earlier. Further, in case of conjugated NPs, transferrin as reported could have masked the recognization sites on the surface of colloidal systems thereby reducing the liver uptake (Litzinger et al. 1994, V. Soni et al., 2008). Opposite trend was observed in case of spleenic uptake. The overall uptake of PTX NPs in comparison to PTX solution increased in the spleen after intravenous administration as depicted in Table 3. This may be attributed to the retention of nanoparticles in the reticular fibre meshwork and the macrophages in red pulp of spleen resulting in high accumulation (Litzinger et al. 1994). These results indicate the major role of liver and spleen in the clearance of drug in solution and nanoparticle formulations.

Table 6. 4: Concentration of PTX in different organs/tissues after i.v. administration to rats at dose of 20mg/kg

Organs/ tissues	Time (hrs)	Concentration (µg/gm of tissue) ± SD					
		PTX solution	PTX PLGA NPs	Pluronic®P85 coated PTX PLGA NPs	Tf conjugated PTX PLGA NPs	PTX PBCA NPs	PTX GTS SLN
Liver	1	322.50 ± 10.32	264.37 ± 6.34	238.13 ± 7.65	202.53 ± 8.46	246.21 ± 6.87	233.75 ± 4.37
	2	276.25 ± 8.45	244.38 ± 8.21	233.18 ± 4.98	173.75 ± 6.73	213.13 ± 9.35	188.13 ± 5.86
	4	204.72 ± 5.30	101.88 ± 9.54	77.52 ± 5.27	89.35 ± 6.91	125.79 ± 6.58	95.63 ± 7.47
	24	26.19 ± 2.34	32.69 ± 1.87	32.58 ± 4.14	36.25 ± 3.25	39.38 ± 1.43	26.23 ± 1.98
Spleen	1	193.33 ± 8.24	226.67 ± 11.43	240.29 ± 9.45	220.52 ± 7.46	201.33 ± 9.19	228.81 ± 8.42
	2	206.61 ± 7.31	243.31 ± 6.39	246.73 ± 5.46	226.67 ± 8.12	216.00 ± 5.48	245.45 ± 5.81
	4	214.25 ± 5.23	246.46 ± 9.24	253.31 ± 7.59	240.00 ± 4.37	235.33 ± 6.32	247.71 ± 3.46
	24	88.17 ± 2.18	90.34 ± 1.31	86.00 ± 1.89	78.63 ± 1.68	70.67 ± 2.35	68.00 ± 3.09
Lung	1	45.61 ± 3.27	57.75 ± 3.86	62.47 ± 2.17	67.50 ± 4.32	62.75 ± 2.95	60.92 ± 3.19
	2	49.26 ± 5.12	61.25 ± 2.98	67.28 ± 3.25	74.75 ± 2.78	67.34 ± 1.43	73.50 ± 2.51
	4	31.48 ± 4.19	52.50 ± 4.35	54.39 ± 2.58	64.78 ± 3.21	57.17 ± 2.76	48.53 ± 2.64
	24	17.52 ± 3.87	24.63 ± 2.69	24.17 ± 1.32	20.56 ± 2.47	25.50 ± 1.24	19.75 ± 1.01
Kidney	1	210.82 ± 10.32	129.85 ± 9.86	122.75 ± 5.78	121.86 ± 8.64	125.36 ± 6.54	117.48 ± 5.25
	2	219.75 ± 9.12	149.28 ± 7.47	145.67 ± 6.72	143.50 ± 6.58	141.28 ± 5.23	135.50 ± 4.18
	4	102.50 ± 8.76	124.64 ± 8.24	133.24 ± 9.31	128.49 ± 5.12	119.50 ± 6.21	110.92 ± 7.54
	24	43.82 ± 9.49	81.50 ± 7.12	85.51 ± 7.43	103.75 ± 3.18	83.64 ± 4.12	79.75 ± 3.46

Organs/ tissues	Time (hrs)	Concentration (µg/gm of tissue) ± SD					
		PTX solution	PTX PLGA NPs	Pluronic®P85 coated PTX PLGA NPs	Tf conjugated PTX PLGA NPs	PTX PBCA NPs	PTX GTS SLN
Heart	1	65.11 ± 4.32	49.33 ± 2.98	44.85 ± 3.42	42.81 ± 5.36	45.33 ± 2.18	43.29 ± 1.97
	2	60.67 ± 3.75	45.63 ± 4.17	41.27 ± 3.20	38.14 ± 2.16	42.18 ± 2.78	37.12 ± 1.02
	4	47.37 ± 1.87	32.17 ± 0.85	35.46 ± 1.03	30.73 ± 2.18	34.19 ± 3.21	27.84 ± 0.96
	24	28.62 ± 3.21	20.18 ± 2.46	17.33 ± 3.10	12.48 ± 2.26	16.73 ± 1.02	14.67 ± 1.26
Tumor	1	8.02 ± 2.13	10.35 ± 1.05	17.49 ± 1.46	19.50 ± 3.14	11.72 ± 2.67	16.43 ± 1.79
	2	13.17 ± 1.39	17.58 ± 2.07	26.50 ± 1.56	32.53 ± 4.32	24.50 ± 1.89	22.64 ± 1.03
	4	10.50 ± 1.86	16.74 ± 3.28	26.08 ± 4.19	30.19 ± 1.76	23.47 ± 3.23	21.28 ± 2.18
	24	0.05 ± 0.01	11.37 ± 1.08	10.26 ± 0.89	18.79 ± 2.14	10.92 ± 1.65	11.39 ± 1.37

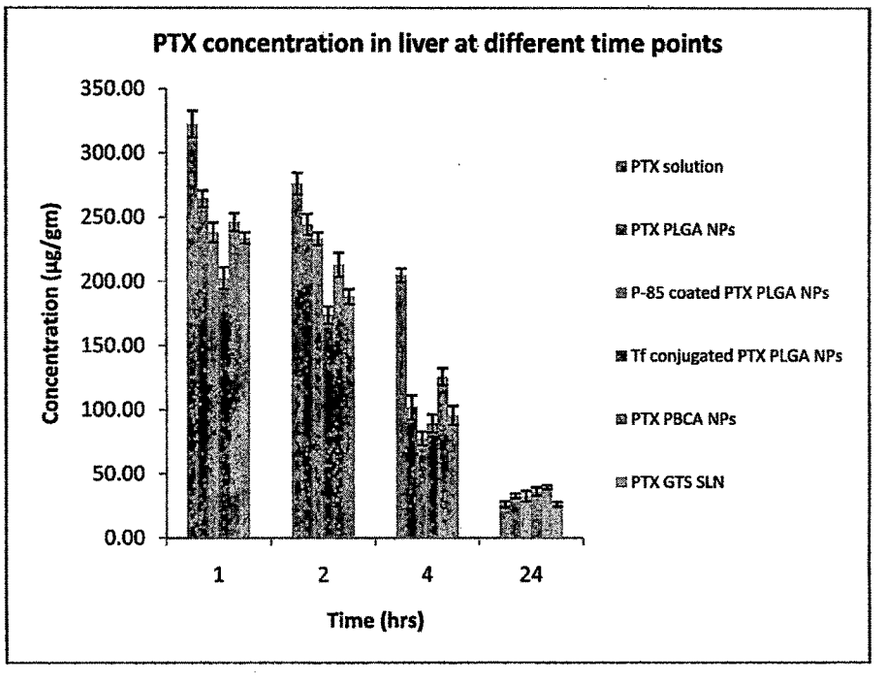

Figure 6. 3: Liver PTX concentrations after i.v. administration in rats at dose of 20mg/kg.

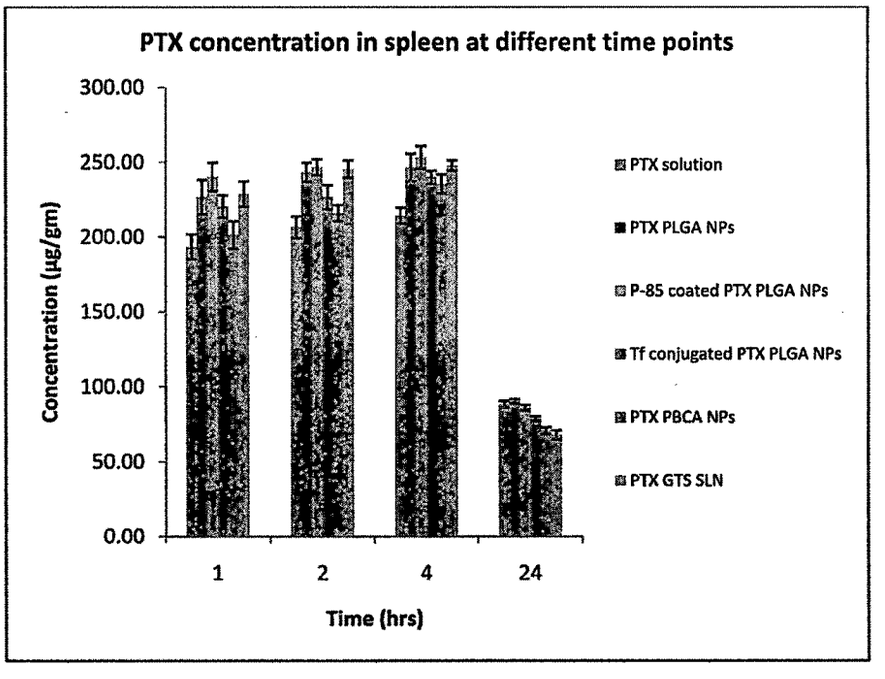

Figure 6. 4: Spleen PTX concentrations after i.v. administration in rats at dose of 20mg/kg.

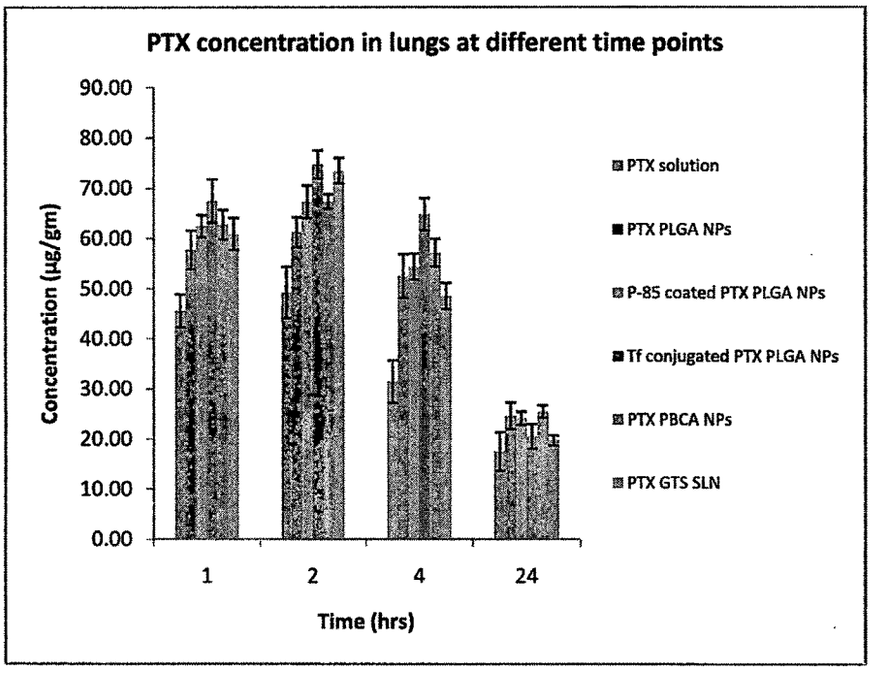

Figure 6. 5: Lung PTX concentrations after i.v. administration in rats at dose of 20mg/kg.

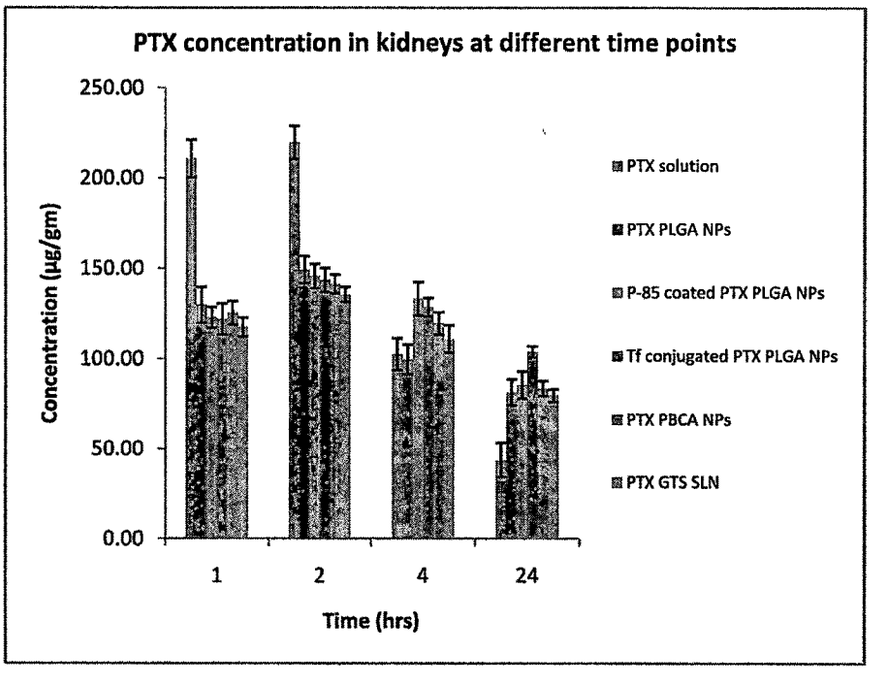

Figure 6. 6: Kidney PTX concentrations after i.v. administration in rats at dose of 20mg/kg.

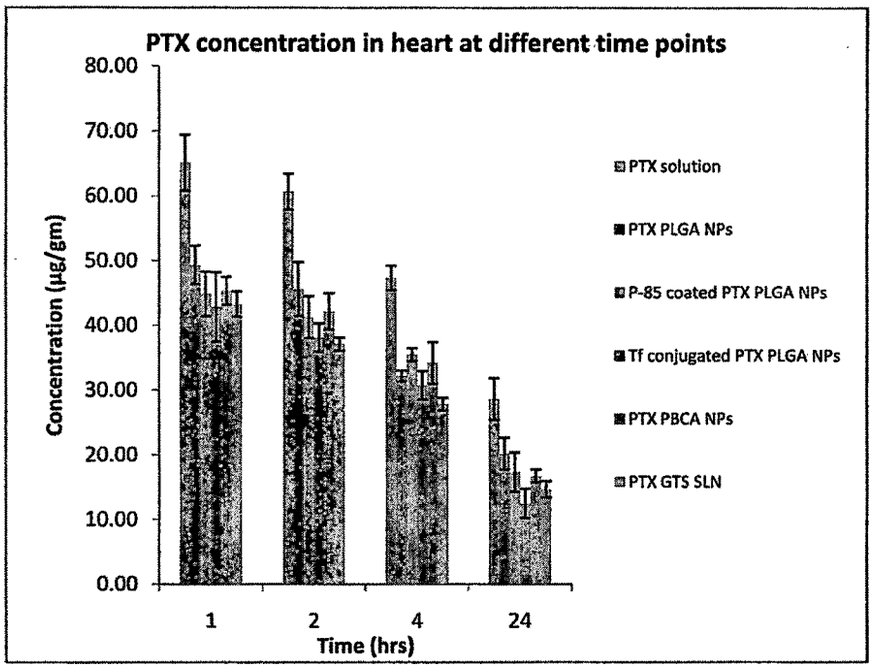

Figure 6. 7: Heart PTX concentrations after i.v. administration in rats at dose of 20mg/kg.

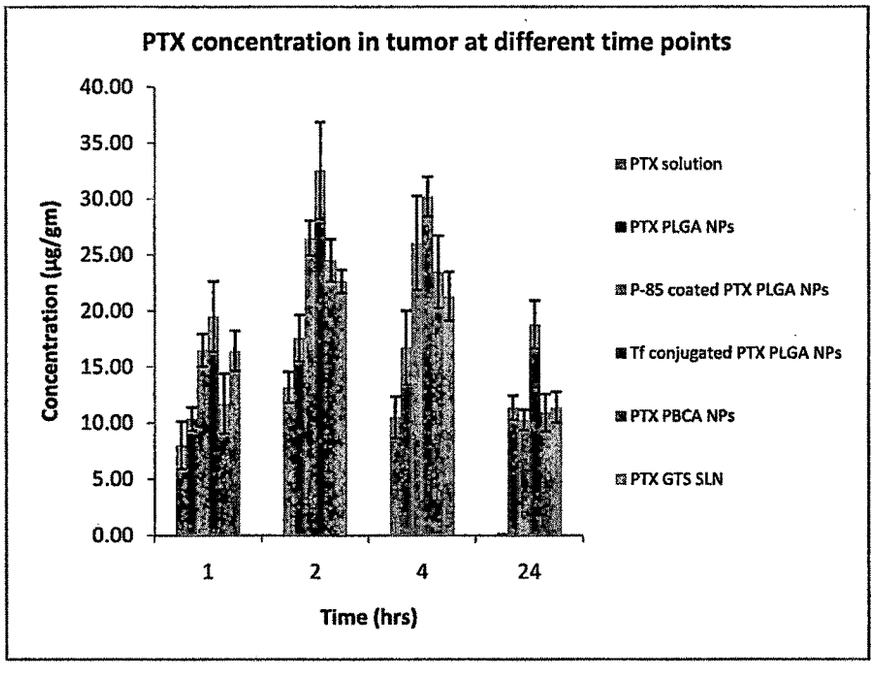

Figure 6. 8: Tumor PTX concentrations after i.v. administration in rats at dose of 20mg/kg.

PTX is mainly metabolized in the kidneys. The distribution pattern of PTX NPs and PTX solution in kidneys indicate higher values for solution than the NPs initially upto 2 hrs due to rapid clearance of PTX in solution which is supported by lower plasma concentrations. At 24 hrs post injection the concentration of PTX in kidneys was more in case of NPs confirming the higher elimination half life for PTX encapsulated in nanoparticles. Also the $t_{1/2}$ for drug in NPs is greater than in solution. The higher accumulation of PTX NPs than PTX solution was observed in the lungs. This enhanced deposition is resulted due to the size of the nanoparticles. The concentration of PTX in heart in case of NPs was significantly lower than that in solution indicating a potential reduction in cardiotoxicity in comparison to the drug solution.

Tumor tissue is the major tissue under investigation in the present study. The distribution profile of PTX solution and NPs in subcutaneous C6 glioma after i.v. administration in rats is shown in Table 3 and tumor AUC $_{(0\rightarrow 24)}$, AUC $_{(0\rightarrow\infty)}$, MRT and $t_{1/2}$ of PTX solution and NPs are presented in Table 4. The tumor accumulation of free PTX was significantly ($p<0.05$) low at all time points in comparison to PTX NPs. PTX in solution gets effluxed out of the C6 glioma cells by Pgp (C6 glioma cells express P-glycoproteins (Pgp) responsible for multidrug resistance) and hence tumor PTX concentration of free PTX is much less than PTX NPs (Lamprecht et al., 2006). When PTX in incorporated into the NPs the Pgp cannot recognise PTX hence it does not get effluxed out. Hence, a greater concentration of PTX in tumor is achieved in case of NPs. Highest concentration of PTX in tumor was found in case of Tf-PTX-PLGA NPs at 2 hrs. This may be due to the active targeting via transferrin (Sahoo et al., 2004). Targeting of anticancer agents via Tf receptors which are over-expressed by 2- to 10-folds in most of the cancer cells have been demonstrated as an effective approach for treatment of multidrug resistant tumors. Increased concentration of PTX in tumor with NPs demonstrates their use in multidrug resistant tumors.

The tumor AUC $_{(0\rightarrow\infty)}$ of PTX-PLGA NPs, Pluronic®P85 coated PTX-PLGA NPs, Tf conjugated PTX-PLGA NPs, PTX-PBCA NPs and PTX-GTS SLN was found to be 6.77, 7.71, 15.79, 8.14 and 8.9 folds higher than PTX solution respectively. The tumor AUC $_{(0\rightarrow\infty)}$ of Pluronic®P85 coated PTX-PLGA NPs and Tf conjugated PTX-PLGA NPs was found to be

1.13 and 2.33 folds higher than PTX-PLGA NPs respectively. The MRT of PTX in tumors in case of PTX-PLGA NPs, Pluronic®P85 coated PTX-PLGA NPs, Tf conjugated PTX-PLGA NPs, PTX-PBCA NPs and PTX-GTS SLN was found to be 6.8, 4.85, 9.03, 5.95 and 7 folds higher than PTX solution respectively. This can be attributed to inhibition of the drug efflux by membrane Pgp. Pluronic®P85 coated NPs show a greater accumulation of PTX in tumour in comparison to uncoated PLGA NPs because of the Pgp inhibitory activity of the Pluronic®P85 (Batrakova et al., 2001). Also in case of PTX PBCA NPs and PTX GTS SLN due to the surface hydrophilicity because of Poloxamer 188 and due to its Pgp inhibitory activity (Batrakova and Kabanov, 2008) a greater concentration of PTX is found in comparison to the solution. Also, polymeric nanoparticles having hydrophilic surface imparts these NPs long circulating properties and decreased opsonisation in the blood. In addition, the plasma half-time of intravenously injected nanoparticles can be relatively long due to limited uptake by the liver and spleen (Lee et al., 2003; Yoo and Park, 2004). This reduced uptake by the liver and spleen has been exploited for the treatment of solid tumors because the prolonged circulation of nanoparticles allows them to accumulate and extravasate within tumor tissue. Extravasation, which allows an enhanced permeation and retention (EPR) effect, is achieved due to the disorganized vascularization and defective vascular architecture induced in rapidly growing cancers (Matusumura and Maeda, 1986). Therefore, drug delivery using polymeric nanoparticles is an effective strategy for passive tumor targeting (Kwon et al 1985; Yokoyama et al., 1990; Hashizume et al., 2000). In case of active targeting via Tf the NPs conjugated to Tf are selectively taken up by the tumor cells by the Tf receptors present on the surface of the tumor cell. Hence, targeting via Tf is an effective strategy for active targeting.

6.5 Conclusions

From the present study we can conclude that PTX loaded polymeric NPs and SLNs can be used to enhance the blood circulation time in comparison to PTX solution. Moreover, NPs and SLNs of PTX retain the drug in the tumor tissue for significantly longer time in comparison to the drug in solution due to the EPR effect and in case of targeted NPs due to the receptor mediated endocytosis. The drug loaded into polymeric NPs and SLNs could be effective in clinical practise for treatment of MDR tumors as the drug is

retained for longer times in the tumor tissue bypassing the Pgp present on the tumor cell membrane in case of C6 rat gliomas.

References

Batrakova EV, Kabanov AV. Pluronic block copolymers: Evolution of drug delivery concept from inert nanocarriers to biological response modifiers. J. Control Rel 130 (2) (2008) 98-106.

Batrakova EV, Li S, Li Y, Alakhov VY, Elmquist WF, Kabanov AV. Distribution kinetics of a micelle-forming block copolymer Pluronic P85. J. Control Release 100 (2004) 389–397.

Batrakova EV, Miller DW, Li S, Alakhov VY, Kabanov AV, Elmquist WF. Pluronic P85 Enhances the Delivery of Digoxin to the Brain: In Vitro and in Vivo Studies. J. Pharmcol and Exp Thera. 296 (2001) 551-557.

Hashizume H, Baluk P, Morikawa S, McLean JW, Thurston G, Roberge S, Jain RK, McDonald DM. Openings between defective endothelial cells explain tumor vessel leakiness. Am. J. Pathol. 156 (2000) 1363–1380.

Hobbs SK, Monsky WL, Yuan F, Roberts WG, Griffith L, Torchilin VP, Jain RK. Regulation of transport pathways in tumor vessels: role of tumor type and microenvironment. Proc. Natl. Acad. Sci. U. S. A. 95 (8) (1998) 4607–4612.

Koziara JM, Whisman TR, Tseng MT, Mumper RJ. In-vivo efficacy of novel paclitaxel nanoparticles in paclitaxel resistant human colorectal tumors. J. Control. Release 112 (2006) 312-319.

Kwon GS, Naito M, Yokoyama M, Okano T, Sakurai Y, Kataoka K. Physical entrapment of adriamycin in AB block copolymer micelles. Pharm. Res. 12 (1995) 192–195.

Lamprecht A, Benoit JP. Etoposide nanocarriers suppress glioma cell growth by intracellular drug delivery and simultaneous P-glycoprotein inhibition. J. Control Release 112 (2006) 208–213.

Lee ES, Shin HJ, Na K, Bae YH. Poly(L-histidine)-PEG block copolymer micelles and pH-induced destabilization. J. Control. Release 90 (2003) 363–374.

Litzinger DC, Buiting AM, Van Rooijen N, Huang L. Effect of liposome size on the circulation time and intra organ distribution of amphipathic poly (ethylene glycol)-containing liposomes. Biochem. Biophys. Acta. 1190 (1994) 99–107.

Maeda H, Wu J, Sawa T, Matsumura Y, Hori K. Tumor vascular permeability and the EPR effect in macromolecular therapeutics: a review. J. Control. Release 65 (2000) 271–284.

Matsumura Y, Maeda H. A new concept for macromolecular therapeutics in cancer chemotherapy: mechanism of tumoritropic accumulation of proteins and antitumor agent smancs. Cancer Res. 46 (1986) 6387–6392.

Moghimi SM, Hedeman H, Muir IS, Illum L, Davis SS. An investigation of the filtration capacity and the fate of large filtered sterically-stabilized microspheres in rat spleen. Biochin. Biophys. Acta 1157 (1993) 233–240.

Moghimi SM, Hunter AC. Poloxamers and poloxamines in nanoparticle engineering and experimental medicine. TibTech October 18 (2000) 413-420.

Muller RH, Mader K, Gohla S. Solid lipid nanoparticles (SLN) for controlled drug delivery—a review of the state of the art. Eur. J. Pharm. Biopharm. 50 (2000) 161–177.

Oyewumi MO, Liu S, Moscow JA, Mumper RJ. Specific association of thiamine-coated gadolinium nanoparticles with human breast cancer cells expressing thiamine transporters, Bioconjug. Chem. 14 (2) (2003) 404–411.

Oyewumi MO, Mumper RJ. Influence of formulation parameters on gadolinium entrapment and tumor cell uptake using folate-coated nanoparticles. Int. J. Pharm. 251 (1–2) (2003) 85–97.

Oyewumi MO, Yokel RA, Jay M, Coakley T, Mumper RJ. Comparison of cell uptake, biodistribution and tumor retention of folatecoated and PEG-coated gadolinium nanoparticles in tumor-bearing mice. J. Control. Release 95 (3) (2004) 613–626.

Sahoo SK, Panyam J, Prabha S, Labhasetwar V. Residual polyvinyl alcohol associated with poly (D,L-lactide-co-glycolide) nanoparticles affects their physical properties and cellular uptake. J. Control Release 82 (2002) 105-114.

Sahoo SK, Wenxue MA, Labhasetwar V. Efficacy of transferrin-conjugated paclitaxel-loaded Nanoparticles in a murine model of prostate cancer. Int. J. Cancer 112 (2004) 335–340.

Soni V, Kohli DV, Jain SK. Transferrin-conjugated liposomal system for improved delivery of 5-fluorouracil to brain. Journal of Drug Targeting 16(1) (2008) 73–78.

Watanabe K, Sakamoto M, Somiya M, Amin R et al., Feasibility and limitations of the rat model by C6 glioma implanted at the subcutaneous region. Neurol Res. 24 (5) (2002) 485-490.

Yokoyama M, Miyauchi M, Yamada N, Okano T, Sakurai Y, Kataoka K, Inoue S. Characterization and anticancer activity of the micelleforming polymeric anticancer drug adriamycin-conjugated poly(ethylene glycol)-poly(aspartic acid) block copolymer. Cancer Res. 50 (1990) 1693–1700.

Yoo HS, Park TG. Folate receptor targeted biodegradable polymeric doxorubicin micelles. J. Control. Release 96 (2004) 273–283.

Yuan F, Dellian M, Fukumura D, Leunig M, Berk DA, Torchilin VP, Jain RK. Vascular permeability in a human tumor xenograft: molecular size dependence and cutoff size, Cancer Res. 55 (17) (1995) 3752–3756.